J. Biochem. 2010;147(3):405–414 doi:10.1093/jb/mvp181

JB THE JOURNAL OF BIOCHEMISTRY

Importance of Tyr310 residue in the third repeat of microtubule binding domain for filament formation of tau protein

Received July 24, 2009; accepted October 22, 2009; published online November 6, 2009

Chisato Nishiura[1], Kengo Takeuchi[1], Katsuhiko Minoura[1,*], Miho Sumida[2], Taizo Taniguchi[2], Koji Tomoo[1,†] and Toshimasa Ishida[1]

[1]Osaka University of Pharmaceutical Sciences, 4-20-1 Nasahara, Takatsuki, Osaka 569-1094; and [2]Behavioral and Medical Sciences Research Consortium, 2-5-7 Tamachi, Akashi, Hyogo 673-0025, Japan

*Katsuhiko Minoura, Osaka University of Pharmaceutical Sciences, 4-20-1 Nasahara, Takatsuki, Osaka 569-1094, Japan, Tel/Fax: +81-726-90-1068; E-mail: minoura@gly.oups.ac.jp

†Koji Tomoo, Osaka University of Pharmaceutical Sciences, 4-20-1 Nasahara, Takatsuki, Osaka 569-1094, Japan, Tel/Fax: +81-726-90-1068; E-mail: tomoo@gly.oups.ac.jp

The inhibition of tau fibrillation is a potential therapeutic target for Alzheimer's and other neurodegenerative diseases. As a series of studies on inhibiting the transition of soluble monomeric tau into mature fibril, the effect of Tyr310 residue in the third repeat (R3) of the microtubule-binding domain (MBD) on the assembly of MBD was investigated using Tyr-substituted MBD mutants by fluorescence, circular dichroism spectroscopy and electron microscopy. Consequently, the importance of the Tyr residue located at position 310, not at other positions, was clearly shown. The conformational comparison of the Tyr310Ala-substituted R3 repeat peptide with the unsubstituted one showed that the Tyr residue contributes to the rigid extended structure of the N-terminal $V^{306}QIVYK^{311}$ sequence, and its replacement by Ala leads to the deformation of the extended structure, consequently losing its aggregation ability. The present results indicate that a compound that interacts specifically with the Tyr residue or an antibody recognizing the region containing the Tyr residue becomes a candidate for inhibiting tau fibrillation.

Keywords: Filament formation/Microtubule-binding domain/Tau/Tyrosine.

Abbreviations: 3RMBD, three-repeated MBD; 4RMBD, four-repeated MBD; AD, Alzheimer's disease; CD, circular dichroism; His, histidine; DQF-COSY, double quantum-filtered chemical shift-correlated spectroscopy; DTT, dithiothreitol; EM, electron microscopy; MBD, microtubule-binding domain; MT, microtubule; NMR, nuclear magnetic resonance; NOESY, nuclear Overhauser effect spectroscopy; PCR, polymerase chain reaction; PHF, paired helical filament; TFE, trifluoroethanol; ThS, thioflavin S; TOCSY, two-dimensional total correlation spectroscopy; TSP, 3-(trimethylsilyl)-propionic acid.

Tau protein is normally found on axonal microtubules (MTs) and plays a role in the regulation of MT formation and stabilization (*1*, *2*). This MT-associated tau is a highly soluble protein and shows hardly any tendency to assemble under physiological conditions. In the brains of Alzheimer's disease (AD) patients, however, tau dissociates from axonal MTs through an extensive phosphorylation and aggregates intracellularly to form the insoluble paired helical filament (PHF) called neurofibrillary tangle (*3*–*5*). Because the degree of dementia in AD patients significantly correlates with the appearance and distribution of this tangle (*6*) and the tau aggregation correlates with the toxicity in cells (*7*), it is important for the prevention and treatment of AD that a method of inhibiting such an abnormal aggregation of the tau protein is developed.

Although the detailed mechanism of the tau self-assembly has not yet been satisfactorily elucidated, it has been clarified that the microtubule-binding domain (MBD) consisting of three or four repeats in the C-terminal half of tau (Fig. 1) assembles into PHF-like filaments (*8*) and constitutes the core structure of PHF (*9*). Previously, we reported that the third repeat (R3) of MBD has the most active function in the *in vitro* filament formation and this is highly related to its amphipathic extended and α-helical conformations at the N-terminal Val306–Lys311 and Leu315–Leu325 sequences, respectively (*10*–*12*). Moreover, to clarify why the self-aggregation ability of the R3 repeat is much higher than that of the R2 repeat (*13*) despite their similar sequences, we examined the effect of the Pro/Lys residue on the self-aggregation of the R2/R3 repeat by their residual exchange, i.e. P312K and K281P mutants, and reported that the potent aggregation ability of R3 is highly related to the conformational disconnection between the extended Val306–Lys311 and helical Leu315–Leu325 sequences blocked by the Pro312 residue (*14*). This indicates that the filament formation of MBD starts from the limited region taking the minimal conformational motif within the R3 repeat.

Then, to clarify which sequence and what type of residue in the R3 repeat is indispensable for the aggregation, in this work, we investigated the function of the Tyr310 residue in the Val306–Lys311 sequence for the MBD filament formation, because this sequence has been associated with filament formation (*15*–*22*) and Tyr is the only aromatic residue in MBD.

The working model of the amphipathic extended Val306–Lys311 plane suggested the orientations of Val306, Ile308 and Tyr310 on the hydrophobic side and the Gln307, Val309 and Lys311 on the hydrophilic

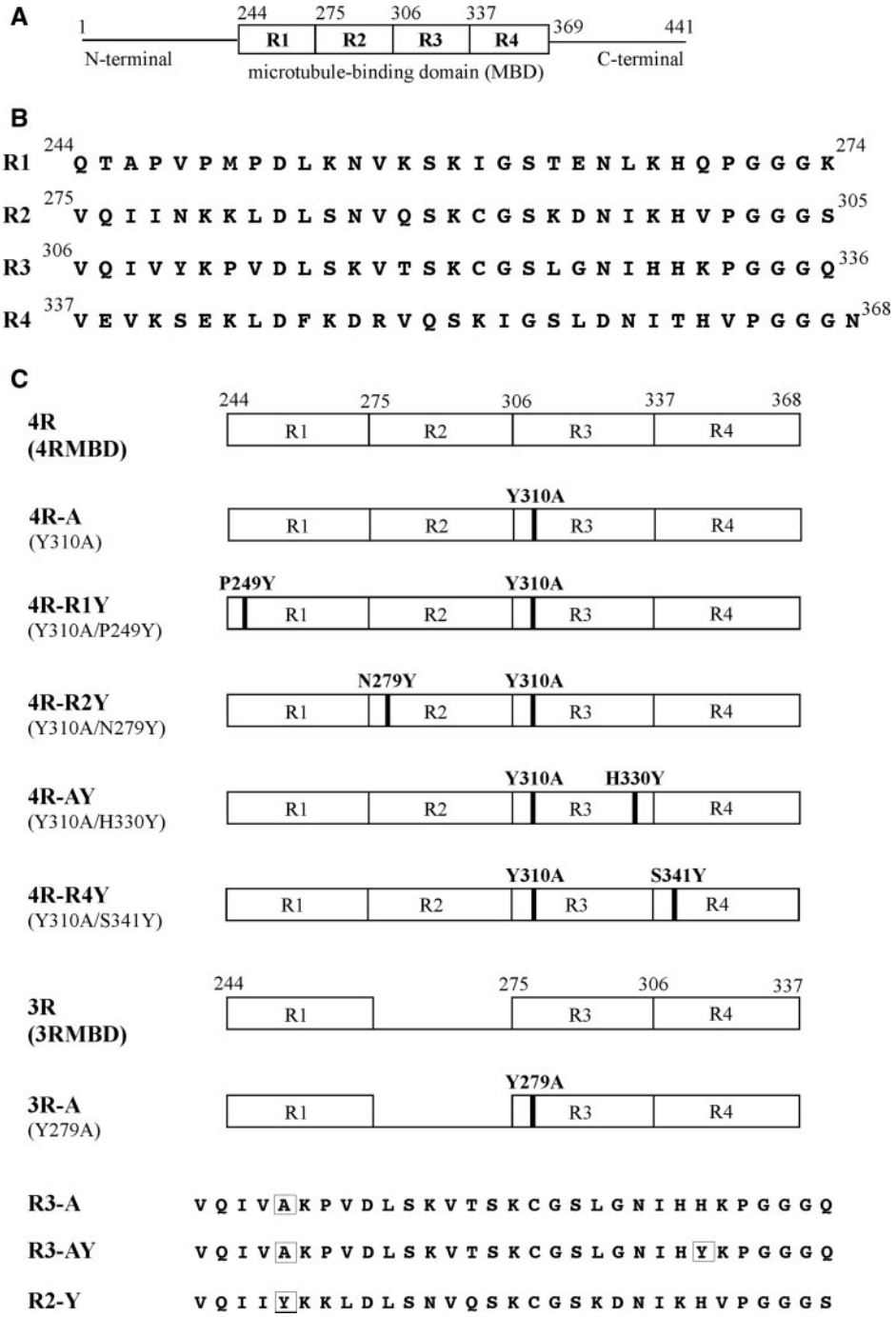

Fig. 1 (A) Schematic of entire four-repeat human tau protein, (B) amino acid sequences of four single-repeat peptides of MBD and (C) Tyr310-substituted mutants used in this work. The letters in parentheses indicate the abbreviation for the corresponding MBD mutants. The number of tau amino acid residue refers to the longest isoform of the human tau protein (441 residues).

side and the stacking in the vertical plane being attributable to the alternating hydrophobic/hydrophilic interactions among the neighbouring planes; a similar schematic has been considered in previous reports (*23*, *24*). To investigate the function of the Tyr310 residue in the MBD filament formation, we investigated the aggregation behaviour of a series of Tyr-substituted, Tyr-deleted or inserted MBD mutants (Fig. 1) by ThS fluorescence, circular dichroism (CD) spectroscopy and electron microscopy (EM). Consequently, it was shown that the filament formation of MBD is largely dependent on the extended structure induced by the Tyr residue, providing useful information for inhibiting the aggregation of tau protein.

Materials and Methods

Peptides and chemicals

R2, R3 and their substituted peptides (R2-Y, R3-A and R3-AY; Fig. 1) were synthesized using a conventional solid-phase synthesizer. The peptides obtained in lyophilized form were characterized by mass

spectrometry and determined to be >95.0% pure by reverse-phase HPLC. Heparin (average molecular weight = 6000) and thioflavin S (ThS) were purchased from Sigma Co. The other commercially available materials used were of reagent grade or higher.

Preparation of recombinant MBD and Tyr-substituted mutants

The gene expression and purification of histidine (His) -tagged three-repeated MBD (3RMBD) and four-repeated MBD (4RMBD) of human brain tau were performed using methods described in a previous paper (*25*), and the purities of these domains were confirmed by SDS–PAGE.

The Tyr-substituted genes of 3RMBD/4RMBD were constructed from human *2N4R* or *2N3R* (*26*) by TA cloning. After amplification by polymerase chain reaction (PCR) using a primer designed for producing each intended gene and rTaq polymerase, each gene was verified by forward and reverse dideoxy sequencings and inserted into the pET-23 vector treated with *Nde*I–*Sal*I restriction enzymes and transformed into the BL21(DE3) strain. The purification of His-tagged MBD mutant was performed using a combination of cation exchange chromatography (HiPrep^{TM} 16/10 SP-FF) [gradient method of sample solution (50 mM Tris-HCl buffer, pH 7.6) by 0–1 M NaCl] and Ni-chelating affinity chromatography (Chelating Sepharose^{TM} Fast Flow) [binding: 50 mM Tris–HCl buffer (pH 7.6) + 0.5 M NaCl + 10 mM imidazole; elution: 50 mM Tris–HCl buffer (pH 7.6) + 0.5 M NaCl + 100 mM imidazole]. The purity of each peptide was confirmed by SDS–PAGE. The concentration of each sample was determined by measuring UV absorption at 280 nm ($\varepsilon = 1280\,mol^{-1}1\,cm^{-1}$ for Tyr residue) and Bradford protein assay (*27*).

ThS fluorescence measurement

The experimental conditions suitable for measuring the heparin-induced aggregation of repeat peptides by ThS fluorescence measurement were previously determined (*13*). Thus, a 25 μM solution of each repeat peptide was prepared using the 50 mM Tris–HCl buffer (pH 7.6), and 10 μM ThS was added to each solution. Fluorescence intensity was measured using a JASCO FP-6500 instrument with a 2 mm quartz cell maintained at 25 C using a circulating water bath. After adding 6.25 μM heparin (optimal concentration for aggregation) to each sample solution, the aggregation profile of each peptide was monitored by plotting the time course of fluorescence intensity with excitation at 440 nm and emission at 500 nm. The background fluorescence of each sample solution was subtracted when necessary. The same measurement was repeated at least three times using newly prepared samples to confirm the reproducibility, and the averaged values were used for the data presentation.

CD measurement

The 25 μM solution of each repeat peptide was prepared using the 20 mM phosphate buffer (pH 7.6). After adding 6.25 μM heparin to each sample solution, the CD spectral change was monitored as a function of the time course of the reaction. All measurements were taken at 25°C with a JASCO J-820 spectrometer in a cuvette with a 2-mm path length. For each experiment under N_2 gas flow, the measurement from 190 to 250 nm was repeated eight times and the results were summed. The same measurement was repeated at least three times using newly prepared samples to confirm the reproducibility of the results. Data are expressed in terms of the mean residual ellipticity (θ) in deg cm^2 $dmol^{-1}$.

^{1}H-nuclear magnetic resonance analyses of R2-Y and R3-A substituted peptides

Each sample was dissolved in water/trifluoroethanol (TFE)-d_2 mixtures of 0–100% TFE content (20% interval). ^{1}H- nuclear magnetic resonance (NMR) spectra were recorded on a Varian unity INOVA 500 spectrometer using a variable temperature-control unit. ^{1}H chemical shifts were referenced to 0 ppm for 3-(trimethylsilyl)-propionic acid (TSP). The NMR measurements were performed under the following conditions: concentration 2 mM, temperature 298 K and pH 4.0. The pH was adjusted by adding HCl or NaOH. Two-dimensional total correlation spectroscopy (TOCSY) and nuclear Overhauser effect spectroscopy (NOESY) were acquired in a phase-sensitive mode using standard pulse programs available in the Varian software library. For the temperature-dependence experiment, the chemical shift of each Cα proton was measured in the range of 15–45°C (10°C intervals).

The proton peak assignments and 3D molecular constructions of R2-Y and R3-A mutants were performed in the same manner as those of R2 and R3 (*10*, *12*). Assuming the same correlation time for all the protons, the offset dependence of NOESY cross peaks was used to estimate the secondary structure of the peptide, where the NOE intensities were classified into three groups (strong, medium and weak). The vicinal coupling constants obtained from double quantum-filtered chemical shift-correlated spectroscopy (DQF-COSY) measurements were used to estimate the possible torsion angles: $^3J_{HN\alpha H} = 1.9–1.4\cos\theta + 6.4\cos^2\theta$, where $\phi = |\theta–60|^\circ$ for the φ torsion angle around the $C'_{i-1}–N_i–C\alpha_i–C'_i$ bond sequence (*28*).

The 3D structures of R2-Y and R3-A in 100% TFE solution that fulfill the NOE distance and *J* torsion angle constraints of intramolecular proton pairs were constructed by dynamic simulated annealing (SA) method using the CNS program (*29*). As the input data for the distance constraint, the proton–proton pairs were classified into three distance groups in accordance with their NOE intensities: strong (1.8–3.0 Å), medium (1.8–4.0 Å) and weak (1.8–5.0 Å). The torsional constraint was applied to φ torsion angle, that is, $-120 \pm 40^\circ$ for $J_{HN\alpha H} > 8$ Hz, $-75 \pm 25^\circ$ for $J_{HN\alpha H} < 6$ Hz and $-100 \pm 60^\circ$ for the others. The RMSD analyses of the energy-minimized structures were carried out using the MOLMOL program (*30*).

Results and Discussion

Y310A mutation inhibits the aggregation of MBD

To investigate the effect of the R3 N-terminal Tyr310 residue on the filament formation of 3RMBD/4RMBD, two Y310A mutants, 4R-A and 3R-A (Fig. 1), were prepared and their filament formation profiles were measured by the ThS fluorescence method. As shown in Fig. 2, both 4RMBD and 3RMBD completely lost the aggregation ability following the Tyr →Ala substitution. This complete loss was also observed under acidic and reducing conditions, although the addition of dithiothreitol (DTT) increases the aggregation ability of 4RMBD significantly (*25*). This shows the contribution of the Tyr residue to the filament formation of MBD.

The CD spectra showed that the inhibition of the heparin-induced filament formation of MBD is caused by the stabilization of the native random conformation by the Tyr → Ala mutation (Fig. 3). It is generally accepted that the initial random conformation of MBD is transformed into a β-strand with the progress of aggregation; the CD spectrum of 4RMBD shows the concomitant transition of random and α-helix structures to β-sheet structure, and that of 3RMBD shows an isochromatic point of two-state conformational transition (*13*). This indicates again the Tyr310 residue-related conformational transition that is necessary for the aggregation of MBD. Similarly, the EM images of 3RMBD and 4RMBD showed the importance of the Tyr310 residue in the filament formation (Fig. 4A).

Positional importance of Tyr residue for filament formation

To investigate the positional importance of Tyr residue in the MBD filament formation, four double-substituted mutants were prepared (Fig. 1), Y310A/H330Y (4R-AY), Y310A/P249Y (4R-R1Y), Y310A/N279Y (4R-R2Y) and Y310A/S341Y (4R-R4Y), and

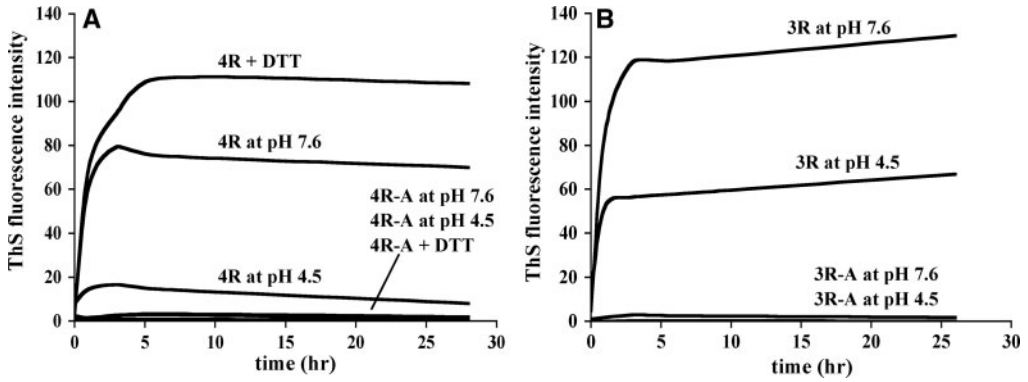

Fig. 2 ThS fluorescence intensity profiles of (A) 4R and 4R-A under neutral, acidic and reducing conditions and of (B) 3R and 3R-A under neutral and acidic conditions. The intensities under acidic and reducing conditions were measured in the 50 mM acetic acid buffer (pH 4.5) and in the 50 mM Tris–HCl buffer (pH 7.6) containing 1 mM DTT, respectively.

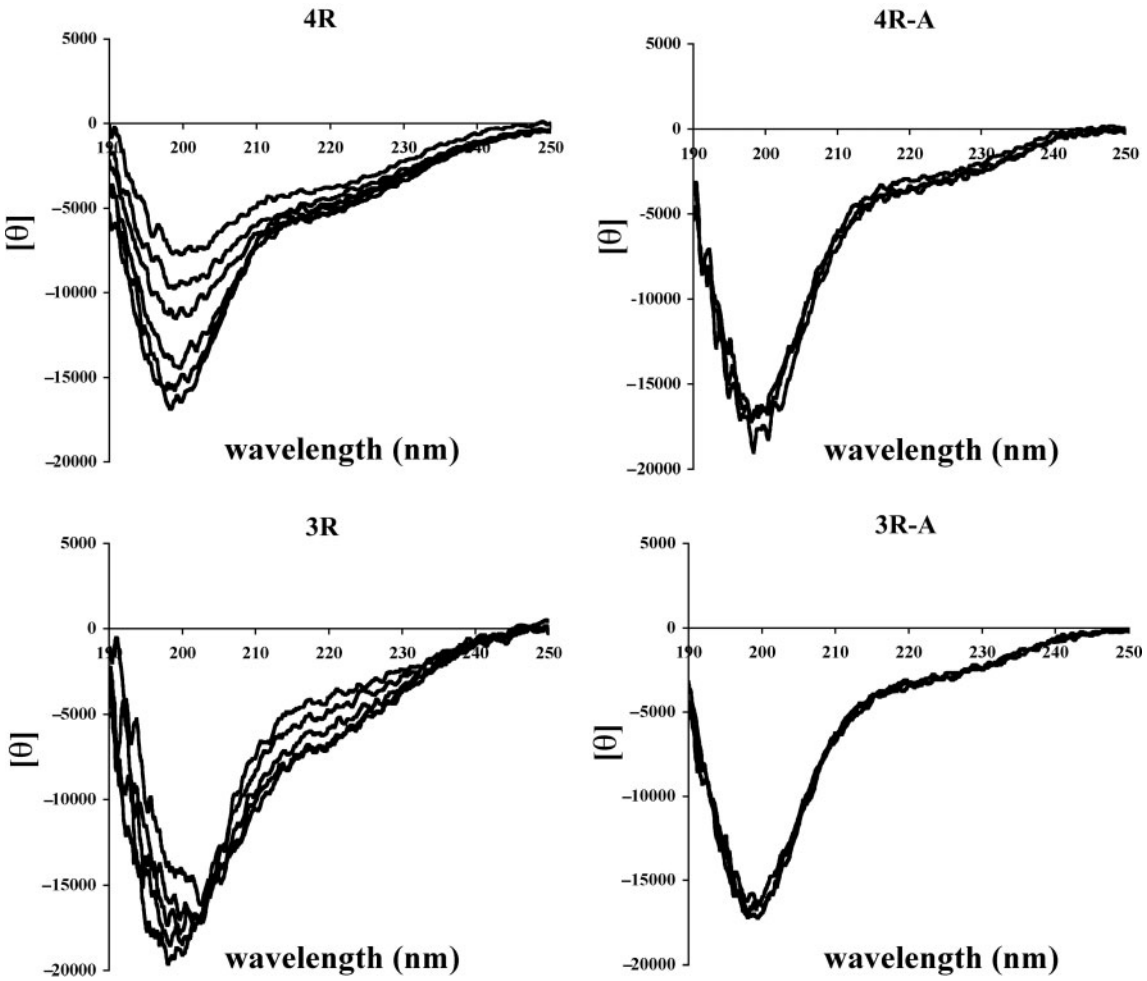

Fig. 3 Time-dependent CD spectral changes of 4R, 4R-A, 3R and 3R-A under neutral condition. The respective CD spectra of 4R and 3R correspond to 0 min, 20 min, 1 h, 3 h, 6 h and 23 h after adding heparin to the solution (horizontal axis from bottom to top at 200 nm).

their aggregation profiles were monitored by fluorescence measurement (Fig. 4C). From these results, the importance of the Tyr residue located at the R3 N-terminal 310 position in the filament formation is obvious. The 4R-AY mutant shows no contribution of the Tyr residue positioned at the R3 C-terminal side to the aggregation, although the sequence around the mutated region is similar to the N-terminal one. Moreover, the Tyr residue located at the R4 N-terminal side also showed no contribution to the aggregation.

In contrast, a notable self-aggregation ability was observed for the 4R-R2Y mutant. Since the N-terminal sequence of the Tyr-replaced R2 repeat

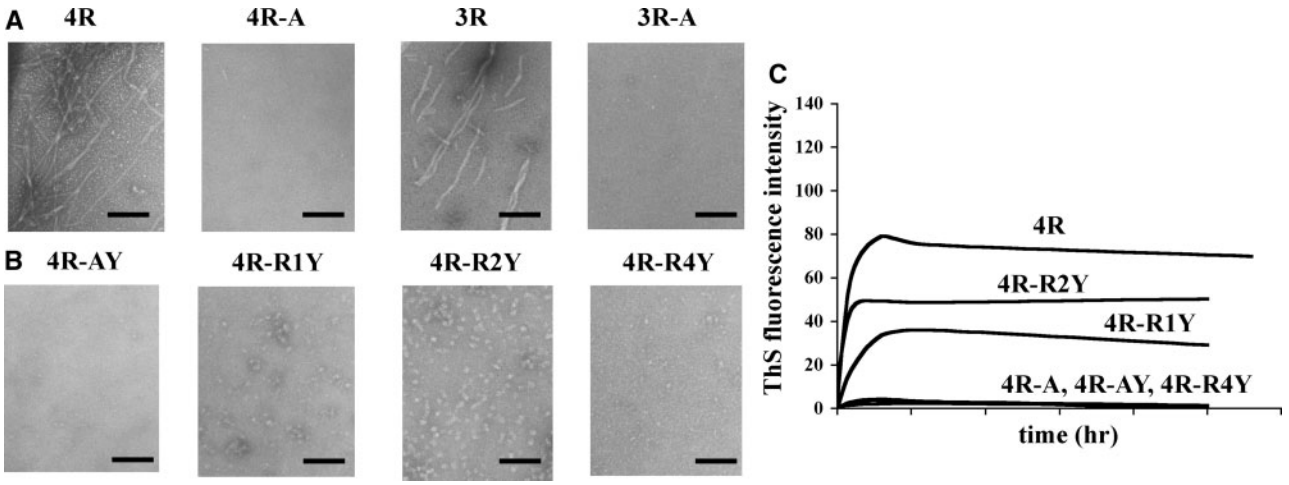

Fig. 4 Negative-staining EM images of (A) 4R, 4R-A, 3R and 3R-A and (B) 4R-AY, 4R-R1Y, 4R-R2Y and 4R-R4Y and (C) ThS fluorescence intensity profiles of 4R, 4R-A, 4R-AY, 4R-R1Y, 4R-R2Y and 4R-R4Y under neutral condition. The length of the bar in (A) and (B) corresponds to 500 nm.

is similar to that of the R3 repeat, this indicates that the N-terminal six sequence of the R3 repeat participates significantly in starting the aggregation of MBD.

The CD spectra of these mutants showed the same random conformations and no notable changes were essentially observed following the addition of heparin (data not shown), although the moderate decrease in the fluorescence intensity at 200 nm was observed for 4R-R1Y and 4R-R2Y with the elapse of the reaction time. This suggests again the close relationship between the Tyr residue and filament formation of MBD.

The EM images of these mutants (Fig. 4B) reflected well the fluorescence and CD spectra results. No notable filaments were formed for all the mutants. However, 4R-R1Y and 4R-R2Y formed globular assemblies, probably the intermediate state of the filament formation, although no such assemblies were formed at all for 4R-AY and 4R-R4Y.

Effect of Tyr substitution on aggregation of R2 and R3 single repeats

To determine whether the marked loss of self-aggregations observed for the Tyr310-substituted MBD mutants resulted only from the R3 single repeat or is dependent on the remaining repeats, the aggregation behaviours of three Tyr-substituted single repeats (R2-Y, R3-A and R3-AY; Fig. 1) were investigated by fluorescence, CD and EM measurements (Fig. 5). The aggregation ability of the R3 repeat was completely lost in the R3-A and the aggregation of its mutant was not recovered by the H330Y mutation (R3-AY), where both mutants maintained the random conformation and did not form any filament; the 10-fold decrease in the filament formation ability of the VQIVYK peptide following the Tyr → Ala substitution has already been reported (*21*). In contrast, the comparison of the fluorescence profiles of R2-Y and R2 shows the increased aggregation ability of R2 by the Gln → Tyr mutation to nearly the same extent as that of R3. Interestingly, the CD spectrum of the R2-Y mutant is similar to that of the R3 repeat but not that of the R2 repeat, indicating that the conformational behaviour accompanied by the aggregation is controlled by the R3 N-terminal sequence. These results clearly suggest that the Tyr310-dependent aggregation of MBD is simulated well by the R3 single repeat.

Conformational comparison of R3/R2 with R3-A/R2-Y in TFE solution

Previously, we reported that (i) the self-assembly of the R3 single repeat, similar to 4RMBD, is most significantly promoted in the Tris–HCl buffer containing ~30% TFE, in which the conformation takes an intermediate transition state from a random structure to an α-helical structure of MBD and (ii) the N-terminal extended structure of the V^{306}QIVYK^{311} sequence and the helical-like structure of the L^{315}SKVTSKC^{322} sequence in the R3 repeat provide a structural trigger for initiating the aggregation (*11*, *12*).

Because the conformational feature of the R3 single repeat in TFE and water has been already clarified (*12*, *31*), the possible relationship between the conformations and filament formation abilities of R3 and R3-A was investigated on the basis of (i) their 3D structures in TFE, (ii) the TFE content-dependent NOE connectivities of their neighbouring protons and (iii) temperature coefficients of Cα protons of their peptides. Although their 3D structures in TFE do not reflect the active structures suitable for the aggregation because of no ThS fluorescence intensity at 100% TFE, it would be useful to estimate the possible conformational feature in the aqueous solution containing ~30 % TFE.

By using the NOE distance and $^{3}J_{\mathrm{HN}C\alpha\mathrm{H}}$ torsion angle constraints of intramolecular proton pairs (Fig. 6A), the 3D structures of R3-A and R2-Y in the TFE solution were constructed by dynamic SA calculations, where the orientations around the Lys6–Pro7 and Lys26–Pro27 ω bonds for R3-A and Val26–Pro27 ω bond for R2-Y were determined to be

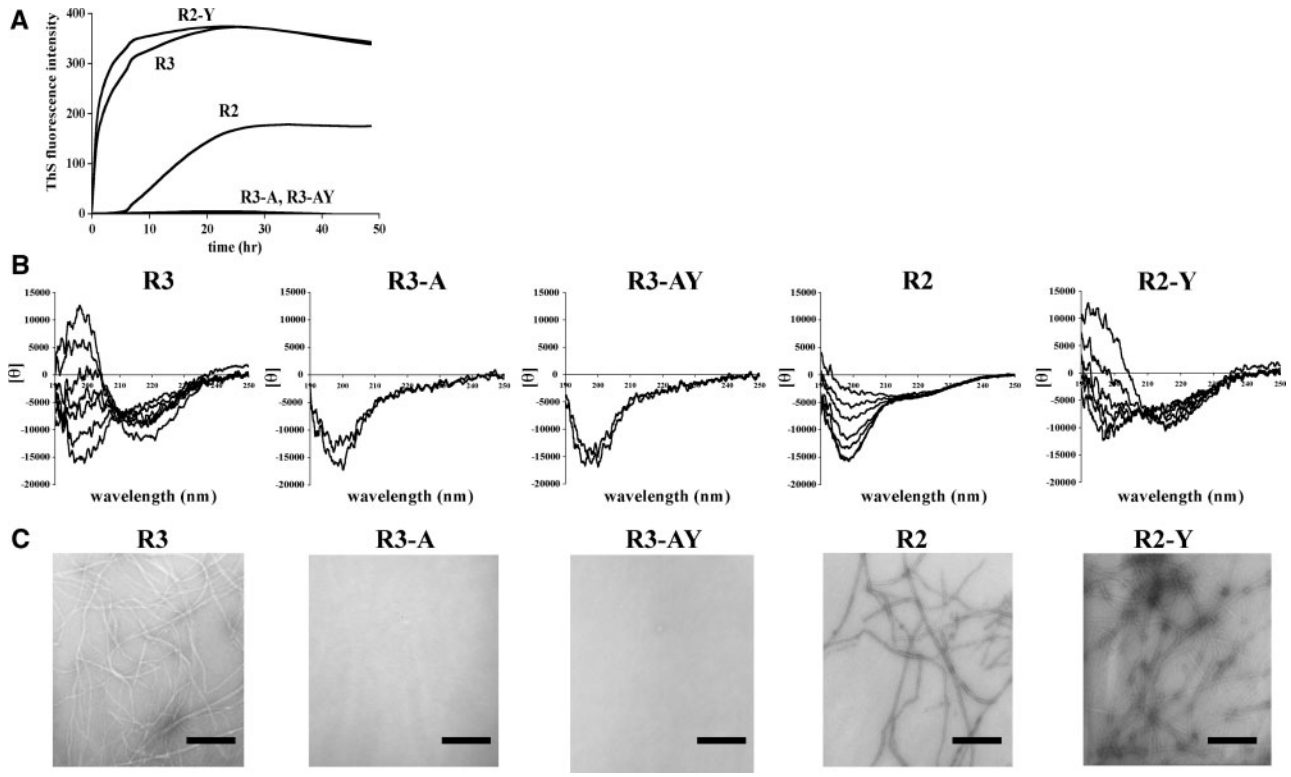

Fig. 5 (A) Time-dependent ThS fluorescence intensity, (B) CD spectral profiles and (C) EM images of R3, R3-A, R3-AY, R2 and R2-Y under neutral condition.

trans from the strong NOEs of the CαH (Lys6/Lys26/Val26)–CδH (Pro7/Pro27) proton pairs. The statistics of the 20 most stable conformers are summarized in Table 1. Their averaged superpositions on the backbone structure, together with those of R3 and R2 (*10*), are shown in Fig. 6B. The N-terminal extended conformation of the Val1–Lys6 sequence in R3 was lost and shifted to a helical structure in R3-A. Conversely, the helical conformation of the Gln2–Lys6 sequence in R2 was lost and shifted to an extended-like structure in R2-Y.

The sequential NOE networks along the backbone protons at different water/TFE ratios showed the continuous conformational changes from a random structure in water to a helical form in TFE solution. Although the respective detailed conformations in the aqueous solution containing ~30% TFE (corresponding to the most activated solution for the self-assembly) were not determined because of few NOE constraints, the significant differences between R3 and R3-A and between R2 and R2-Y could be observed at their N-terminal sequences. The N-terminal VQIVYK sequence of R3 showed the $^{3}J_{\mathrm{HNC\alpha H}}$ values of >8 Hz, indicating the rigid and extended conformation (Table 2). A similar extended conformation could be estimated for the $^{3}J_{\mathrm{HNC\alpha H}}$ values (7–8 Hz) of the N-terminal VQIIY sequence of R2-Y. In contrast, the $^{3}J_{\mathrm{HNC\alpha H}}$ values were >7 Hz for the N-terminal VQIVAK and VQIINK sequences of R3-A and R2, indicating the TFE content-dependent conformational change. On the other hand, the $d_{\alpha N(i,i+3)}$ and $d_{\alpha\beta(i,i+3)}$ NOE cross peaks showed the formation of a similar helical structure at the Ser11–Cys17 sequence with the increase in TFE content.

To estimate the structural rigidity of the N-terminal sequence for the peptides with Tyr residue, the change of CαH chemical shifts was measured as a function of temperature (Fig. 7). The N-terminal sequences of R3 and R2-Y showed small slope ($\Delta\delta/\Delta T$) values, compared with those of R3-A and R2, suggesting the rigid conformation of R3 and R2-Y N-terminal regions.

The present results suggested that the Y310A mutant shifts the rigid extended conformation of the R3 N-terminal VQIVYK sequence to the relatively flexible conformation, resulting in the loss of the aggregation ability of the R3 repeat. The opposite behaviour was observed between R2 and R2-Y. It is also notable that the random structure of the Leu10–Cys17 sequence in water is transformed to a helical structure without being affected by Tyr → Ala mutation. Thus, the structural requirement for the potent aggregation ability of the R3/R2-Y repeat is in the cooperative contribution of the TFE-content-independent extended rigid structure of the N-terminal Val1–Lys5 sequence and the TFE-content-dependent α-helical structure of the Ser11–Cys17 sequence.

General discussion on role of Tyr310 residue in tau filament formation

Although the mechanism of the tau PHF formation has not yet been satisfactorily elucidated, the important contribution of the R3 N-terminal V^{306}QIVYK^{311} sequence in MBD has been sufficiently determined

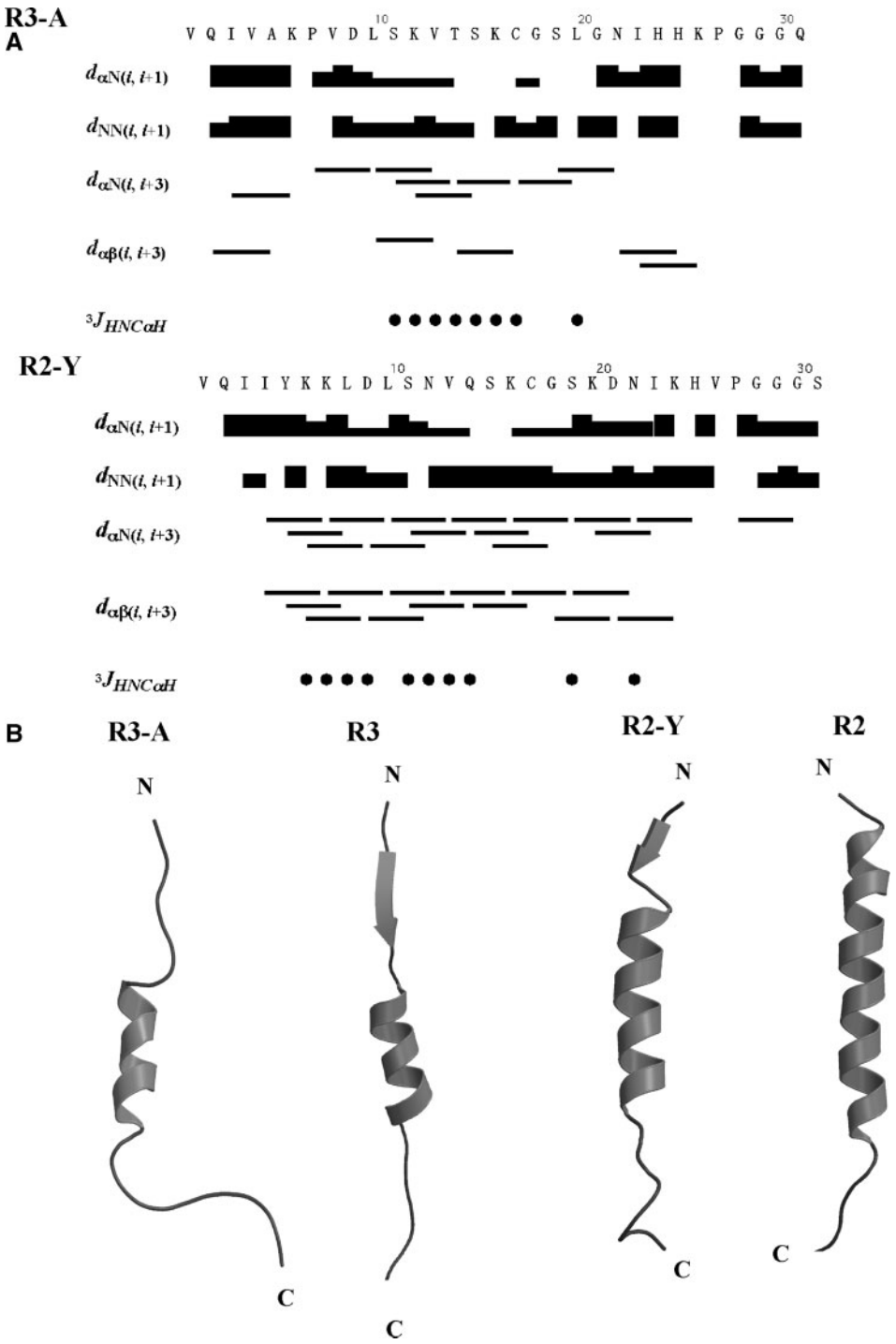

Fig. 6 (A) Diagrams of NOE connectivity between the neighbouring protons along the backbone chain of R3-A and R2-Y ($d_{\alpha N,(i,i+1)}$, $d_{NN(i,i+1)}$, $d_{\alpha N(i,i+3)}$ and $d_{\alpha\beta(i,i+3)}$) in TFE and (B) comparison of averaged backbone conformations commonly observed in various NMR conformers of R3-A with R3 and R2-Y with R2. The observed NOE intensity is represented by the thickness of each bar. Residues with $^3J_{HNC\alpha H} < 6$ Hz are indicated by circles. The N- and C-terminal regions in (B) correspond to the upper and lower sides, respectively.

(*15*–*22*). Because of its amphipathic extended structure, it would be reasonable to consider the stacking in the vertical plane attributable to the alternating hydrophobic/hydrophilic interactions through the locations of Val306/Ile308/Tyr310 residues on the hydrophobic plane and Gln307/Val309/Lys311 residues on the hydrophilic plane, as the major contribution of this sequence to the filament formation. In this work, to investigate the role of Tyr310 residue in the VQIVYK sequence, several Tyr-substituted and Tyr-inserted mutants were prepared and their filament behaviours were investigated by ThS fluorescence, CD and EM measurements. Consequently, it was shown that (i) the Tyr residue and its location at the 310 position are essential for the filament formations of 3RMBD and 4RMBD, (ii) the marked decrease in

Table 1. Structural statistics of 20 stable structures.

	R3-A	R2-Y
Number of structures	20	20
Number of constraints:		
Total number of NOEs	245	318
Intraresidue NOEs	125	198
Sequential NOEs	99	89
Inter-residue NOEs	21	31
Dihedral angles	24	28
RMS deviation (N, Cα, C′)(Å)	. . . 0.52(*19*)[a]	0.56(*17*)[b]
RMS deviation from NOE (Å)	0.058(*2*)	0.042(*1*)
NOE violations >0.10Å	6.2(*1*)	3(*1*)
Energy (kcal/mol)		
Overall	182(*7*)	108(*4*)
NOE	161(*5*)	39(*2*)
Angle	56(*2*)	46(*2*)
Bond	11(*1*)	7(*1*)
Improper	12(*1*)	3(*2*)
van der Waals	41(*3*)	12(*2*)

[a]Calculated from residues 10 to 20. [b]Calculated from residues 7 to 20.

Table 2. Comparison of $^3J_{HNC\alpha H}$ values of N-terminal sequences.

	J/Hz			
Residue number	R3	R3-A	R2	R2-Y
1	n.d.[a]	n.d.	n.d.	n.d.
2	n.d.	n.d.	n.d.	n.d.
3	8.2	6.8	6.3	7.8
4	8.8	6.7	5.6	7.4
5	8.4	6.8	5.1	7.2
6	8.2	6.6	4.8	5.9
7	n.d.	n.d.	4.6	5.8
8	7.6	6.2	4.8	5.5
9	7.5	6.2	5.0	5.0
10	6.6	6.4	4.5	6.2

[a]Not detected.

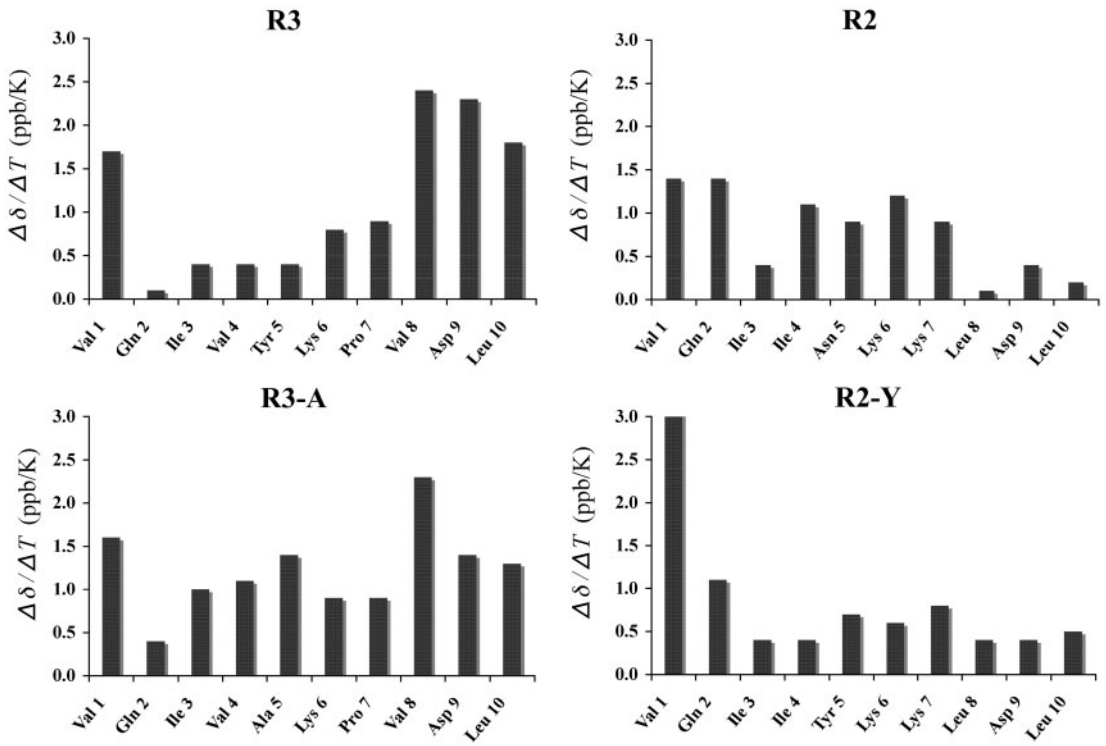

Fig. 7 Temperature coefficients of Cα protons of N-terminal sequences of R3, R3-A, R2 and R2-Y. The chemical shift of each Cα proton was measured in the range of 15°C to 45°C with an interval of 10°C.

the aggregation ability by Y310A mutation in the MBD results from the complete loss of the aggregation ability of the R3 repeat and (iii) its aggregation loss is mainly due to the deformation of the rigid and extended structure of the N-terminal VQIVAK sequence, because the increased aggregation ability of the R2-Y mutant is due to the reconstruction of the extended structure of the N-terminal sequence. These results indicate that the Tyr310 residue plays a vital role in forming the extended structure of the R3 N-terminal sequence, which is indispensable for the aggregation of MBD. The importance of π–π stacking of aromatic rings has been considered to promote the formation of filamentous or fibrillar aggregates by polypeptides (*32*, *33*). Thus, this additional role of Tyr310 may be importantly concerned in forming the filament formation via the extended structure of R3 N-terminal.

The work was carried out with the tau fragments, i.e. MBD and its repeat peptides. Thus, it is important to discuss whether the present results are also valid for the intact full-length tau, because the aggregation behaviour of the tau short fragment peptide does not necessarily coincide with that of the intact tau protein (*34*). Concerning the assembly between the full-length tau and its MBD fragment, however, it has been reported (*15*, *17*, *35*, *36*) that the spectroscopic and morphological properties of the heparin-induced tau assembly could be monitored well by MBD; the aggregated 4RMBD has the typical PHF ultrastructure, the double-stranded twisted appearance with a cross-over repeat of ~80 nm (*25*), which is similar to that of full-length tau protein (*35*). Also the full-length tau lacking the third repeat moiety decreases the ability of self-assembly, similar to the case of 4RMBD (*34*). Thus, the present result suggests that the compound or antibody that can specifically block the function of the Tyr310 residue becomes a potent inhibitor of the tau PHF formation.

Funding

Grants-in-aid for scientific research from the Ministry of Education, Culture, Sports, Science, and Technology of Japan.

Conflict of interest

None declared.

References

1. Goedert, M., Jakes, R., Spillantini, M.G., and Crowther, R.A. (1994) *Microtubules* (Hyams, J.S. and Lloyd, C.W., eds.), pp. 183–200, Wiley-Liss, New York
2. Delacourte, A. and Buee L. (1997) Normal and pathological tau proteins as factors for microtubule assembly. *Int. Rev. Cytol.* **171**, 167–224
3. Goedert, M. and Spillantini, M.G. (2000) Tau mutations in frontotemporal dementia FTDP-17 and their relevance for Alzheimer's disease. *Biochim. Biophys. Acta* **1502**, 110–121
4. Johnson, G.V. and Hartigan, J.A. (1999) Related tau protein in normal and Alzheimer's disease brain. *J. Alzheimers Dis.* **45**, 329–351
5. Goedert, M., Spillantini, M.G., Hasegawa, M., Jakes, R., Crowther, R.A., and Klug, A. (1996) Molecular dissection of the neurofibrillary lesions of Alzheimer's disease. *Cold Spring Harb. Symp. Quant. Biol.* **61**, 565–573
6. Braak, H. and Braak, E (1991) Neuropathological staging of Alzheimer-related changes. *Acta NeuroPathol* **82**, 239–259
7. Bandyopadhyay, B., Li, G., Yin, H., and Kuret, J. (2007) Tau aggregation and toxicity in a cell culture model of tauopathy. *J. Biol. Chem.* **282**, 16454–16464
8. Crowther, R.A., Olesen, O.F., Jakes, R., and Goedert, M. (1992) The microtubule binding repeats of tau protein assemble into filaments like those found in Alzheimer's disease. *FEBS Lett.* **309**, 199–202
9. Wischik, C.M., Novak, M., Thogersen, H.C., Edwards, P.C., Runswick, M.J., Jakes, R., Walker, J.E., Milstein, C., Roth, M., and Klug, A. (1988) Isolation of a fragment of tau derived from the core of the paired helical filament of Alzheimer disease. *Proc. Natl Acad. Sci. USA* **85**, 4506–4510
10. Minoura, K., Yao, T.-M., Tomoo, K., Sumida, M., Sasaki, M., Taniguchi, T., and Ishida, T. (2004) Different associational and conformational behaviors between the second and third repeat fragments in the tau microtubule-binding domain. *Eur. J. Biochem.* **271**, 545–552
11. Hiraoka, S., Yao, T.-M., Minoura, K., Tomoo, K., Sumida, M., Taniguchi, T., and Ishida, T. (2004) Conformational transition state is responsible for assembly of microtubule-binding domain of tau protein. *Biochem. Biophys. Res. Commun.* **315**, 659–663
12. Minoura, K., Mizushima, F., Tokimasa, M., Hiraoka, S., Tomoo, K., Sumida, M., Taniguchi, T., and Ishida, T. (2005) Structural evaluation of conformational transition state responsible for self-assembly of tau microtubule-binding domain. *Biochem. Biophys. Res. Commun.* **327**, 1100–1104
13. Mizushima, F., Minoura, K., Tomoo, K., Sumida, M., Taniguchi, T., and Ishida, T. (2006) Fluorescence-coupled CD conformational monitoring of filament formation of tau microtubule-binding repeat domain. *Biochem. Biophys. Res. Commun.* **343**, 712–778
14. Tokimasa, M., Minoura, K., Hiraoka, S., Tomoo, K., Sumida, M., Taniguchi, T., and Ishida, T. (2005) Importance of local structures of second and third repeat fragments of microtubule-binding domain for tau filament formation. *FEBS Lett.* **579**, 3481–3486
15. Von Bergen, M., Friedhoff, P., Biernat, J., Heberle, J., Mandelkow, E.M., and Mandelkow, E. (2000) Assembly of tau protein into Alzheimer paired helical filaments depends on a local sequence motif ((306)VQIVYK(311)) forming beta structure. *Proc. Natl Acad. Sci. USA* **97**, 5129–5134
16. Perez, M., Santa-Maria, I., Tortosa, E., Cuadros, R., Valle, M.D., Hernandez, F., Moreno, J., and Avila, J. (2007) The role of the VQIVYK peptide in tau protein phosphorylation. *J. Neurochem.* **103**, 1447–1460
17. Mocanu, M.M., Nissen, A., Eckermann, K., Khlistunova, I., Biernat, J., Drexler, D., Petrova, O., Schonig, K., Bujard, H., Mandelkow, E., Zhou, L., Rune, G., and Mandelkow, E.M. (2008) The potential for β-structure in the repeat domain of tau protein determines aggregation, synaptic decay, neuronal loss, and coassembly with endogeneous tau in inducible mouse models of tauopathy. *J. Neurosci.* **28**, 737–748
18. Margittai, M. and Langen, R. (2006) Side chain-dependent stacking modulates tau filament structure. *J. Biol. Chem.* **281**, 37820–37827
19. Eliezer, D., Barre, P., Kobaslija, M., Chan, D., Li, X., and Heend, L. (2005) Residual structure in the repeat

domain of tau: echoes of microtubule binding and paired helical filament formation. *Biochemistry* **44**, 1026–1036
20. Andrones, O.C., Von Bergen, M., Biernat, J., Seidel, K., Griesinger, C., Mandelkow, E., and Baldus, M. (2008) Characterization of Alzheimer's-like paired helical filaments from the core domain of tau protein using solid-state NMR spectroscopy. *J. Am. Chem. Soc.* **130**, 5922–5928
21. Goux, W.J., Kopplin, L., Nguyen, A.D., Leak, K., Rutkofsky, M., Shanmuganandam, V.D., Sharma, D., Inouye, H., and Kirschner, D.A. (2004) The formation of straight and twisted filaments from short tau peptides. *J. Biol. Chem.* **279**, 26868–26875
22. Inouye, H., Sharma, D., Goux, W.J., and Kirschner, D.A. (2006) Structure of core domain of fibril-forming PHF/tau fragments. *Biophys. J.* **90**, 1774–1789
23. Von Bergen, M., Barghorn, S., Li, L., Marx, A., Biernt, J., Mandelkow, E.M., and Mandelkow, E. (2001) Mutations of tau protein in front temporal dementia promote aggregation of paired helical filaments by enhancing local beta-structure. *J. Biol. Chem.* **276**, 48165–48174
24. Gamblin, T.C. (2005) Potential structure/function relationships of predicted secondary structural elements of tau. *Biochim. Biophys. Acta* **1739**, 140–149
25. Yao, T.-M., Tomoo, K., Ishida, T., Hasegawa, H., Sasaki, M., and Taniguchi, T. (2003) Aggregation analysis of the microtubule-binding domain in tau protein by spectroscopic methods. *J. Biochem.* **134**, 91–99
26. Goedert, M., Spillantini, M.G., Jakes, R., Rutherford, D., and Growther, R.A. (1989) Multiple isoforms of human microtubule-associated protein tau: sequences and localization in neurofibrillary tangles of Alzheimer's disease. *Neuron* **3**, 519–526
27. Bradford, M.M. (1976) A rapid and sensitive method for the quantitation of microgram quatities of protein utilizing the principle of protein dye binding. *Anal. Biochem.* **72**, 248–254
28. Bystrov, V.F. (1976) Spin–spin coupling and the conformational states of peptide systems. *Prog. Nucl. Magn. Reson. Spectrosc.* **10**, 41–81
29. Brunger, A.T., Adams, P.D., Clore, G.M., DeLano, W.L., Gros, P., Grosse-Kunstleve, R.W., Jiang, J.S., Kuszewski, J., Nilges, M., Pannu, N.S., Read, R.J., Rice, L.M., Simonson, T., and Warren, G.L. (1998) Crystallography and NMR system: a new software suited for macromolecular structure determination. *Acta Crystallogr.* **D54**, 905–921
30. Koradi, R., Billeter, M., and Wuthrich, K. (1996) MOLMOL: a program for display and analysis of macromolecular structures. *J. Mol. Graph.* **14**, 51–55
31. Minoura, K., Tomoo, K., Ishida, I., Hasegawa, H., Sasaki, M., and Taniguchi, T. (2003) Solvent-dependent conformation of the third repeat fragment in the microtubule-binding domain of tau protein, analyzed by ^{1}H-NMR spectroscopy and molecular modeling calculation. *Bull. Chem. Soc. Jpn.* **76**, 1617–1624
32. Gazit, E. (2002) A possible role for π-stacking in the self-assembly of amyloid fibrils. *FASEB J.* **16**, 77–83
33. Inouye, H., Shatma, D., Goux, W. J., and Kirschner, D. A. (2006) Structure of core domain of fibril-forming PHF/Tau fragments. *Biophys. J.* **90**, 1774–1789
34. Santa-Maria, I., Perez, M., Hernandez, F., Munoz, V., Moreno, F.J., and Avila, J. (2006) In vitro tau fibrillization: mapping protein regions. *Biochim. Biophys. Acta* **1762**, 683–692
35. Friedhoff, P., Von Bergen, M., Mandelkow, E.M., and Mandelkow, E. (2000) Structure of tau protein and assembly into paired helical filaments. *Biochim. Biophys. Acta* **1502**, 122–132
36. Perez, M., Valpuesta, J.M., Medina, M., Montejo de Garcini, E., and Avila, J. (1996) Polumerization of tau into filaments in the presence of heparin: the minimal sequence required for tau–tau interaction. *J. Neurochem.* **67**, 1183–1190